AIP Advances

Influence of deposition temperature of thermal ALD deposited Al2O3 films on silicon surface passivation

Neha Batra, Jhuma Gope, Vandana, Jagannath Panigrahi, Rajbir Singh, and P. K. Singh

Citation: AIP Advances **5**, 067113 (2015); doi: 10.1063/1.4922267
View online: http://dx.doi.org/10.1063/1.4922267
View Table of Contents: http://scitation.aip.org/content/aip/journal/adva/5/6?ver=pdfcov
Published by the AIP Publishing

Influence of deposition temperature of thermal ALD deposited Al_2O_3 films on silicon surface passivation

Neha Batra,[1,2] Jhuma Gope,[2] Vandana,[2] Jagannath Panigrahi,[1,2] Rajbir Singh,[1,2] and P. K. Singh[1,2]
[1]*Academy of Scientific & Innovative Research (AcSIR), CSIR-National Physical Laboratory (CSIR-NPL) Campus, New Delhi-110012, India*
[2]*Silicon Solar Cell Group (Network of Institutes for Solar Energy) CSIR-NPL, New Delhi-110012, India*

(Received 3 February 2015; accepted 24 May 2015; published online 5 June 2015)

The effect of deposition temperature (T_{dep}) and subsequent annealing time (t_{anl}) of atomic layer deposited aluminum oxide (Al_2O3) films on silicon surface passivation (in terms of surface recombination velocity, SRV) is investigated. The pristine samples (as-deposited) show presence of positive fixed charges, Q_F. The interface defect density (D_{it}) decreases with increase in T_{dep} which further decreases with t_{anl} up to 100s. An effective surface passivation (SRV<8 cm/s) is realized for $T_{dep} \geq 200$ °C. The present investigation suggests that low thermal budget processing provides the same quality of passivation as realized by high thermal budget process (t_{anl} between 10 to 30 min). [http://dx.doi.org/10.1063/1.4922267]

I. INTRODUCTION

Silicon (Si) is the most widely used substrate for solar cell applications due to its well established technology.[1,2] The solar cell efficiency is limited due to several losses such as lattice thermalisation loss, sub-band gap loss, looses associated with electrical contacts, recombination loss etc. The recombination losses occur both in the bulk region as well as at the semiconductor surface (due to dangling bonds).[3] To make the solar cell economically viable, one way is to reduce the Si wafer thickness (in terms of gm/W usages and simultaneously increase in device efficiency). In thinner wafers, both surfaces are close to area of carrier generation and their collection and therefore, are prone to enhanced recombination losses which have detrimental effect on device performance. The losses at the semiconductor interfaces or surfaces can be suppressed by surface passivation for which two strategies exist and are well appraised in literature. The first strategy is based on the reduction of the density of electronic states at the surface and the second is based on significant reduction of one type of charge (electron/hole) carrier from the surface by an internal electric field.[4–10] The interface defect density can be reduced by chemical route where atomic hydrogen or a halogen atom is, generally, attached with the unsaturated Si (dangling) bonds. Consequently surface is passivated[11] and this process is referred as chemical passivation. On the other hand, fixed charges (both in bulk and at interface) present in a dielectric layer repel the charges of same polarity at the Si interface deep into the bulk Si and consequently the recombination of the photo-generated carriers reduces. This is called field-effect passivation. An excellent surface passivation is a prerequisite for realization of next-generation high efficiency silicon solar cells. Minority carrier lifetime is the measure of surface passivation effectiveness and is generally quantified in terms of surface recombination velocity (SRV) which can be deduced from the measured minority carrier lifetime (τ_{eff}).

Thermally grown silicon di-oxide (SiO_2) is most widely used for silicon surface passivation which requires high temperature processing. In this situation, bulk lifetime degradation associated with high thermal budget cannot be ruled out.[12] Besides SiO_2, other dielectric layers such Si_xN_y:H, SiC and a-Si:H are also used for surface passivation.[13] Recently, aluminum oxide (Al_2O3)

films show high quality surface passivation for both n- and p-Si.[5–7,9] Al_2O_3, a dielectric, has large band gap (8.8 eV) and its films have excellent thermal and chemical stability and good adhesion with silicon.[14–16] Al_2O_3 films can be deposited by several techniques such as molecular beam epitaxy (MBE),[17] chemical vapor deposition (CVD),[18–20] plasma enhanced chemical vapor deposition (PECVD),[21,22] sputtering[23] and atomic layer deposition (ALD).[4–7,9,24] ALD being a conformal deposition process provides high-quality thin films with precise control over the thickness.[9,25]

The best reported SRV values for Al_2O_3 films deposited by ALD process are made by suitable combination of deposition temperature; $T_{dep} \geq 200$ °C and post deposition annealing temperature (T_{anl}) between 400-450 °C with annealing time (t_{anl}) in the range 10 to 30 min.[4–7] However, these studies are scattered and are made on different type and quality materials with high thermal budget. However, literature in low thermal budget annealing process using RTP with less annealing time is very few.[9,26]

In this paper, a systematic study is made wherein Al_2O3 films are deposited using thermal ALD process at different deposition temperature. The influence of T_{dep} on silicon surface passivation properties is investigated. Low thermal budget rapid thermal process (RTP) is used to optimize the post deposition annealing time at a fixed annealing temperature (= 400 °C) and the minority carrier lifetime is measured to see the role of the process parameters on surface passivation. Capacitance-voltage (C-V) and X-ray photoelectron spectroscopy (XPS) measurements are performed to understand the mechanism of surface passivation.

II. EXPERIMENTAL DETAILS

Al_2O_3 films are grown on float zone (FZ) chemically mechanically polished (CMP) <100> oriented n-type single crystalline silicon of 5 ± 0.5 Ωcm resistivity having 325 ± 10 μm thickness. To ensure identical surface, electronic and optical properties; the samples are cut from the 100 mm diameter silicon wafer using laser scriber (YAG-50 series, M/s Argus, China). Each sample is a quarter of the larger wafer. The samples are cleaned in piranha solution (H_2SO_4:H_2O2 :: 4:1 by volume) for 15 min followed by dip in 5% HF solution for 2 min.

The films are deposited in thermal ALD reactor (Model: R200, M/s Picosun, Finland) using trimethylaluminum [TMA, $Al(CH_3)_3$] (M/s SAFC, Hitech, UK) and H_2O as precursors for aluminum and oxygen sources respectively. Each deposition cycle consists of two half cycles; one TMA pulse and one H_2O pulse and each step is separated by a nitrogen purge to remove un-reacted excessive precursors. The desired layer thickness can be obtained simply by repeating the number of ALD cycles. The surface chemistry during the first and the second half cycles of thermal ALD process can be described by the following equations respectively.[27]

$$1^{st} \text{ half cycle:} \quad Al-OH + Al(CH_3)_3 \rightarrow Al-O-Al(CH_3)_2 + CH_4 \tag{1}$$

$$2^{nd} \text{ half cycle:} \quad Al-O-Al(CH_3)_2 + 2H_2O \rightarrow Al-O-Al(OH)_2 + 2CH_4 \tag{2}$$

Al_2O_3 films are deposited on one side (for C-V) as well as on both the sides (for lifetime) of the wafer for a fixed number of precursors cycles (= 300) with the deposition temperature variation (= 100 °C, 200 °C and 300 °C; and the samples are denoted as S_{100}, S_{200} and S_{300} respectively). The films are annealed at 400 °C for different annealing time (t_{anl} = 90 s, 105 s and 120 s) in nitrogen (N_2) ambient using rapid thermal process (RTP Model: AS-one 150, M/s Annealsys, France).

The thickness (d_{Al2O3}) and refractive index (n_{Al2O3}) of the films are measured by spectroscopic ellipsometer (Model: M2000, M/s J.A. Wollam Co. Inc., USA). Minority carrier lifetime is measured by two different techniques; Sinton's lifetime tester (Model: WCT-120, M/s Sinton Inc., USA) and microwave photoconductance decay technique (μ-PCD, Model: WT 2000 PV, M/s Semilab Zrt, Hungary). In the first technique, injection level dependence (Δn) of τ_{eff} in a large range ($10^{13} < \Delta n < 10^{16}$ cm^{-3}) is measured that gives an average value of the parameter whereas μ-PCD operates at a fixed injection level ($\sim 1.2 \times 10^{13}$ cm^{-3}). However, the advantage of μ-PCD is that it gives the τ_{eff} map, from which the uniformity of lifetime across the sample surface could be seen. Both the systems give almost comparable τ_{eff} provided the injection levels are matched.[10] Fourier transform infrared spectroscopy (FTIR, Model 2000, M/s Perkin Elmer spectrometer, USA) is used

to know the different bonding configurations in the film. The spectra are recorded in absorption mode. C-V measurements are carried out to find out the interface properties of Al_2O_3/Si and the data is used to evaluate flat-band voltage (V_{FB}), fixed charge density (Q_F) and interface defect density (D_{it}). For C-V measurements, the metal-insulator-semiconductor (MIS) structure is made by depositing aluminum dots (area ~ 0.02cm^2) through a shadow mask on the front side and fully covered back side using an e-beam evaporation system (M/s Hind Hivac, India) and the measurements are done with an impedance/gain phase analyzer (Model: 1260, M/s Solartron, UK) at 1 MHz. XPS measurements (Model: 0520, M/s Omicron nanotechnology) are carried out to do surface analysis and to get information about the bonding that may provide vital information about the surface passivation mechanism. The system is operated at a base pressure of 10^{-11} mbar, where spectra are recorded using Mg-K_α as an X-ray source.

III. RESULTS AND DISCUSSIONS

Film thickness and Refractive index

The film thickness and refractive index of as-deposited samples S_{100}, S_{200} and S_{300} are given in Table I. To check the thickness homogeneity, d_{Al2O3} are measured at different locations on the samples. The variation in d_{Al2O3} across the sample (from edge to center) is less than ±1%. This shows that the films are highly uniform. Table I show the d_{Al2O3} and n_{Al2O3} of as-deposited samples deposited at different T_{dep} for fixed 300 cycles along with the estimated errors. It can be seen that d_{Al2O3} increases with T_{dep}. This is due to the dependence of the reaction kinetics on deposition temperature. At low T_{dep}, growth rate is slow due to slower reaction kinetics primarily associated with thermal activation barrier.[28,29] The refractive index also increases from 1.50 to 1.62 with increase in the deposition temperature. Increase in n_{Al2O3} may be due to the dense and compact films at higher temperature. The refractive index of S_{100} is low in comparison to the films S_{200} and S_{300}. It is reported that at lower deposition temperature, the hydroxyl surface coverage on Al_2O_3 surface is high which may results in the lower density of the film.[27] The low refractive index of a film as compared to its bulk counterpart may be either due to small film thickness or low mass density or the combination of the two. At lower temperature, the decrease in n_{Al2O3} may be attributed to decreased density and to increased impurity levels in films.[30] It is to be noted that in thinner Al_2O_3 films (~ 7 nm), deposited by ALD at 300 °C, n_{Al2O3} ~ 1.5 is observed.[9] This indicates that the lower n_{Al2O3} of S_{100} vis-à-vis S_{200} or S_{300} is primarily due to lower mass density.

Minority carrier lifetime

As mentioned earlier that the minority carrier lifetime is the key parameter to know the quality of passivation. The measured effective carrier lifetime (τ_{eff}) value has contributions from the bulk (τ_{bulk}) and the two wafer surfaces (τ_s) of the silicon sample and these two parameters are related with τ_{eff} as[31,32]

$$\frac{1}{\tau_{eff}} = \frac{1}{\tau_{bulk}} + \frac{1}{\tau_s} \tag{3}$$

where, $\tau_s = W^2/(D\chi_m)$. χ_m are the roots of the transcendental equation $\chi_m \tan(\chi_m) = S_{eff}W/D$ where the subscript m represents the mth root and; D and W are the diffusion constant and thickness of

TABLE I. Thickness (d_{Al2O3}) and refractive index (n_{Al2O3}) of as deposited samples: S_{100}, S_{200} and S_{300}. These values have ~1% measurement uncertainty.

Sample	T_{dep} (°C)	d_{Al2O3} (nm)	n_{Al2O3}
S_{100}	100	24.0	1.50
S_{200}	200	28.4	1.59
S_{300}	300	30.1	1.62

TABLE II. Measured minority carrier lifetime (τ_{eff}) and surface recombination velocity (SRV) values for as-deposited and annealed samples of S_{100}, S_{200} and S_{300}, at an injection level, $\Delta n = 1 \times 10^{15} cm^{-3}$. The measurement uncertainty in τ_{eff} (μs) and SRV (cm/s) values is ~4 %.

			Annealed					
	As-deposited		t_{anl} =90s		t_{anl} =105s		t_{anl} =120s	
Sample	τ_{eff}	**SRV**	τ_{eff}	**SRV**	τ_{eff}	**SRV**	τ_{eff}	**SRV**
S_{100}	584	27.8	440	36.9	360	45.1	304	53.4
S_{200}	588	27.6	1398	11.6	2274	7.1	1856	8.7
S_{300}	824	19.7	1696	9.6	2063	7.9	1853	8.8

the wafer, respectively. S_{eff} is surface recombination velocity (SRV). Amongst the various modes associated with Eq. (3), the fundamental mode (m= 1) is the most significant and the contribution of the higher modes is significantly small and could not be detected experimentally. In this case the above equation reduces to where $\tau_s = W/2S_{eff}$. The factor 2 accounts for the contribution of both surfaces. For very large bulk lifetime, $\tau_{eff} \cong \tau_s$ and in this case the upper limit of SRV ($S_{eff\,max}$) can be estimated using the following relation:

$$S_{eff,\,max} = \frac{W}{2\tau_{eff}} \tag{4}$$

For τ_{eff} measurements, symmetrically passivated samples are prepared by depositing Al_2O_3 films of the same thickness on both sides of the substrates. In Table II, measured τ_{eff} values and corresponding $S_{eff,max}$ of as-deposited and annealed samples of S_{100}, S_{200} and S_{300} at $\Delta n = 1 \times 10^{15}$ cm^{-3} are given. In case of annealed samples, annealing time is varied (t_{anl} = 90 s, 105 s and 120 s) whereas the annealing temperature is fixed at 400 °C. It is observed that the τ_{eff} values of as-deposited samples of S_{100} and S_{200} is almost the same (584 μs and 588 μs respectively) within the measurement uncertainty but in S_{300}, τ_{eff} is increased to 824 μs with increase in T_{dep}. A systematic decrease in τ_{eff} values with the rise in t_{anl} is observed in S_{100}. This decrease in τ_{eff} may be due to the lower density (T_{dep} = 100 °C) structure of the as-deposited film that may not be an effective passivation layer and therefore, results in low value of τ_{eff} after annealing. This observation can be corroborated with the C-V data of the annealed film discussed later. On the other hand, τ_{eff} increases with t_{anl} from 90 s to 105 s in S_{200} and S_{300} and with further increase in t_{anl} (~120 s), τ_{eff} decreases from its maximum. It can be seen from Table II that maximum τ_{eff} (~2274 μs) is observed in S_{200} with t_{anl} = 105 s. This corresponds to SRV ~7 cm/s which is close to S_{300} sample within measurement error. All these results demonstrate that deposition temperature and post-deposition annealing both play important role for surface passivation.[33–38] Figure 1 shows the SRV (at $\Delta n = 1 \times 10^{15}$ cm^{-3}) as a function of t_{anl} of as-deposited and annealed (t_{anl} = 90 s, 105 s, 120 s) samples of S_{100}, S_{200} and S_{300}. The minimum SRV value (~7 cm/s) obtained using low thermal budget RTP process is quite comparable to the values realized with high thermal budget.[4–7] Though, similar annealing time is required to achieve SRV ~7 cm/s for S_{200} and S_{300} but the thermal effective budget of S_{300} is more than S_{200} due to higher T_{dep} (for the fixed t_{anl} and T_{anl}).

Figure 2 shows the injection level dependent τ_{eff} for as-deposited and annealed samples of S_{200} for different t_{anl}. The minority carrier lifetime results illustrate quality surface passivation in the entire range of Δn. Figure 3 shows the τ_{eff} map of the as-deposited and annealed samples (S_{200}) where the four samples (quarter pieces) are put together for the mapping using μ-PCD in order to provide an idea about the uniformity of passivation in the samples.

FTIR Spectroscopy

Figure 4(a) shows the FTIR spectra of as-deposited samples (S_{100}, S_{200} and S_{300}) in absorption mode. All the absorption bands are marked with arrows. The broad absorption band in the range of 400-750 cm^{-1} is attributed to the mixed contributions of Al-O bending and stretching modes

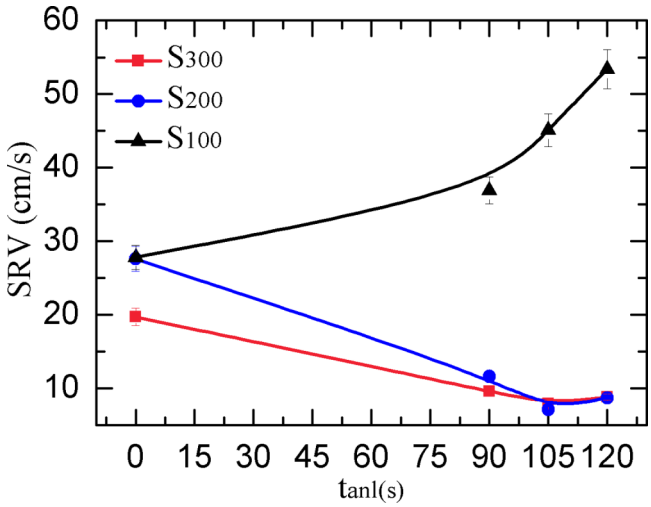

FIG. 1. Calculated surface recombination velocity (SRV) as a function of annealing time (t_{anl}) for as-deposited and annealed samples ($0 \leq t_{anl} \leq 120$ s) of S_{100}, S_{200} and S_{300}.

for both AlO_4 and AlO_6.[39] The absorption peak at 513 cm^{-1} is attributed to Al-O stretching mode of condensed AlO_6.[40] Absorption peaks at 653 cm^{-1} and 700 cm^{-1} are also dominated by O-Al-O bending and Al-O stretching for AlO_6, respectively.[39] Katamreddy et al.[41] have reported that the absence of the peak at 530 cm^{-1} due to Al-O stretching in condensed AlO_6 octahedra indicates the amorphous structure of the film. Similar observations are made in our samples also. A small hump observed in the range 1075-1150 cm^{-1} may be attributed to Si-O-Si symmetric stretching mode.[40,41] This indicates towards the formation of ultra thin layer of SiO_2 at the Al_2O_3/Si interface. The appearance of absorption peak at ~ 1395 cm^{-1} owe their existence to Al=O stretch bands.[42] The absorption bands seen in the range 2340-2360 cm^{-1} are due to carbonate species in the films. The band at ~ 2360 cm^{-1} is assigned to CO_2, bonded to strong Lewis sites of alumina.[43]

Figure 4(b) shows the FTIR spectra of as-deposited and annealed samples of S_{200} at different t_{anl} in the range of 400-2500 cm^{-1}. The absorption peak at 513 cm^{-1} in the as-deposited film broadens after annealing at different temperatures (t_{anl} = 90 s, 105 s and 120 s). The peak observed at 675 cm^{-1} in as-deposited sample is shifted to 710 cm^{-1} in case of annealed samples which is attributed to Al-O stretching for AlO_6. The annealed films also show absorption peak at 1395 cm^{-1}.

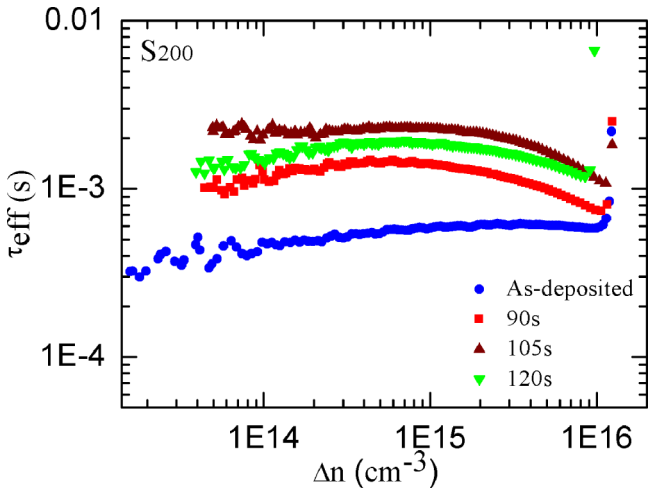

FIG. 2. Measured minority carrier lifetime (τ_{eff}) as a function of injection level (Δn) of as-deposited and annealed (t_{anl} = 90, 105 and 120 s; T_{anl} = 400 °C) sample of S_{200}.

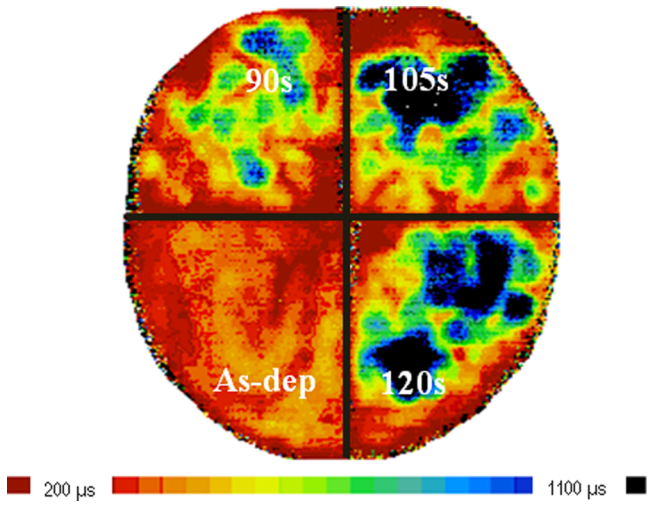

FIG. 3. The map of minority carrier lifetime of as-deposited and annealed (T_{anl} = 400 °C) samples for different time duration (t_{anl} = 90, 105 and 120 s) of S_{200}.

In the annealed films, the peaks at 2340 cm^{-1} and 2360 cm^{-1} is less intense as compared to as-deposited films. Similar results are also obtained for S_{100} and S_{300}.

Capacitance-Voltage (C-V) measurements

Capacitance-Voltage (C-V) measurement is generally used to assess the dielectric property of a material. C-V measurements are performed on MIS structure at 1 MHz frequency. The applied bias voltage (V_G) is varied from negative to positive which shifts the C-V curve from inversion to accumulation region (forward sweep). These measurements are performed to extract the fixed charge polarity and density (Q_F), which is responsible for field effect passivation. Figure 5(a) shows the normalized C-V curves for as-deposited samples. The C-V curves for the as-deposited samples shift towards negative voltages with decrease in deposition temperature. The magnitude of shifting increases with decrease in deposition temperature which suggests that fixed charges also increases with reducing T_{dep}. The fixed charge density is calculated using eq. (5)

$$Q_F = (\varphi_{ms} - V_{FB})C_{OX} \tag{5}$$

where φ_{ms} is the work function difference between metal and semiconductor, V_{FB} is flat band voltage which is extracted from C-V curve and C_{OX} is oxide capacitance of the film. The Q_F of

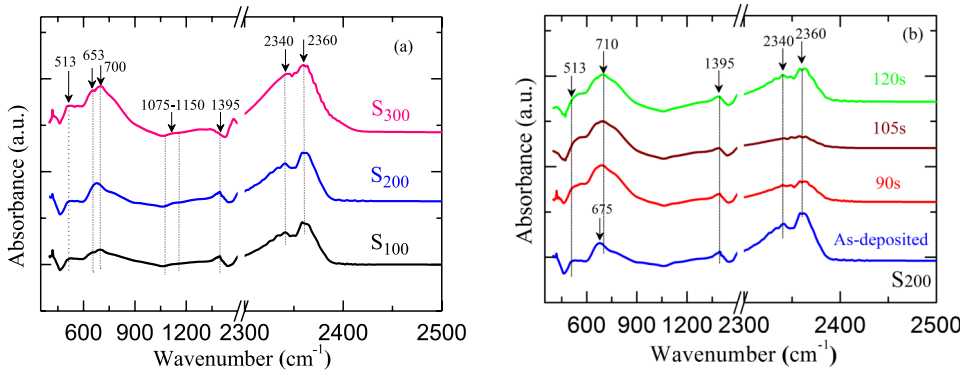

FIG. 4. (a) FTIR spectra of as-deposited samples of S_{100}, S_{200} and S_{300}. (b) FTIR spectra of as-deposited and annealed sample S_{200}, (t_{anl} = 90, 105 and 120 s; T_{anl} = 400 °C).

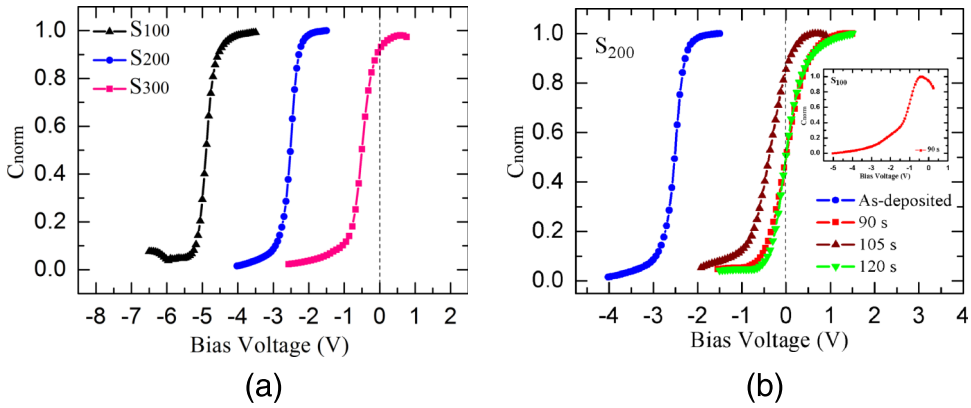

FIG. 5. (a) Normalized C-V curves for as-deposited samples of S_{100}, S_{200} and S_{300} at 1MHz frequency. (b) Normalized C-V curves for as-deposited and annealed samples of S_{200} at 1MHz frequency (t_{anl} = 90, 105 and 120 s; T_{anl} = 400 °C). Inset shows normalized C-V curve of annealed (t_{anl} = 90 s) film of S_{100}.

as-deposited films is positive which are listed in Table III. Rafi et al.[36] also observed positive fixed charges in the Al_2O_3 films deposited at 100 °C.

Figure 5(b) shows the normalized C-V curves for as-deposited and annealed samples (at t_{anl} = 90 s, 105 s, 120 s) of S_{200}. A shift towards less negative voltages in C-V curves with respect to its as-deposited curve is observed with annealing. The calculated values of Q_F are negative (Table III) which confirms that there is an activation of negative fixed charges in these films. The density and polarity of fixed charges are related to the deposition process of oxide films and is associated with local non-stoichiometry or structural defects.[4,9,24,44] It can be seen that with increase in t_{anl} from 90 s to 105 s, value of Q_F decreases and thereafter for t_{anl} = 120 s, the values start increasing. Inset of Fig. 5(b) shows a representative C-V curve of annealed (t_{anl} = 90 s) film of S_{100}. The drop in capacitance value in accumulation region and stretching of the curve indicates towards degradation in the film quality after annealing. This observation is rather surprising and needs further probing. The interface defect density (D_{it}) at Al_2O_3/Si interface can be extracted from the conductance measurements (C-f) and the calculated values (for all as-deposited and annealed samples of S_{200}) are listed in Table III. It is observed that the value of D_{it} decreases with the increase in T_{dep}. The lower value of D_{it} for as-deposited sample S_{300} is primarily responsible for the high value of τ_{eff}. It is well established that in thermal ALD, chemical passivation is dominant which is quantized in terms of D_{it}.[45] Further, the D_{it} value decreases with annealing from 4.2×10^{12} to 1.3×10^{12} $eV^{-1}cm^{-2}$ for t_{anl} from 90 s to 105 s for S_{200}. Henceforth for an increase in annealing duration to 120 s, D_{it} increases. The lowest D_{it} value is observed for sample S_{200} annealed at t_{anl} = 105 s. It is known that the surface passivation is governed primarily by both Q_F and D_{it}. The effective surface passivation requires high Q_F and low D_{it} values. As the two parameters have opposite trend, a trade-off between the two decodes the lowest SRV. In the present case, the maximum τ_{eff} or minimum SRV are realized at t_{anl} = 105 s (S_{200}). C-V measurements reveal that the Al_2O_3/Si

TABLE III. Fixed charge density (Q_F) and interface defect density (D_{it}) of as deposited samples (S_{100}, S_{200} and S_{300}) and annealed samples of S_{200} (t_{anl} = 90 s, 105 s and 120 s; T_{anl} = 400 °C).

Sample	**Q_F($\times 10^{12}$cm^{-2})**	**D_{it}($\times 10^{12}$states/eVcm^2)**
S_{100}	5.42	5.1
S_{200}	2.10	4.2
S_{300}	0.36	3.0
S_{200}(t_{anl} =90s)	-1.27	2.4
S_{200}(t_{anl} =105s)	-0.35	1.3
S_{200}(t_{anl} =120s)	-0.92	1.9

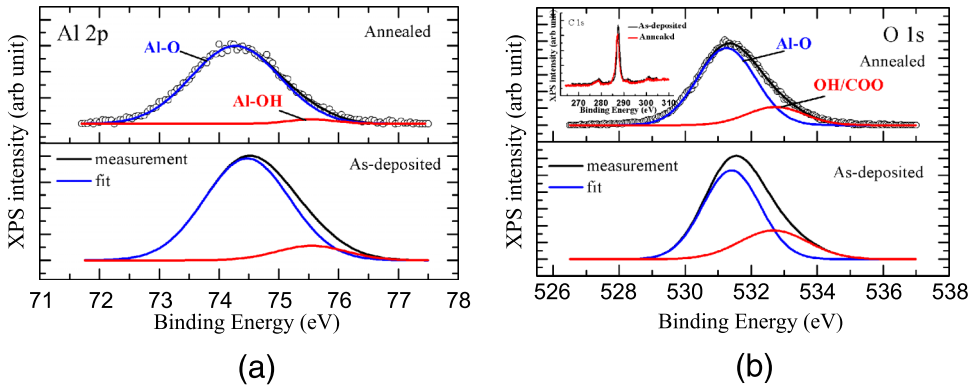

FIG. 6. (a) Deconvoluted Al 2p core level spectra of as-deposited and annealed sample of S_{200}. (t_{anl} = 105 s, T_{anl} = 400 °C). The peak decomposition into Al-O (blue) and Al-OH (red) are indicated. The measured data is shown by black (hollow) circles and the resulting fitted curve is shown by black line. (b) Deconvoluted O 1s core level spectra of as-deposited and annealed sample of S_{200}. (t_{anl} = 105 s, T_{anl} = 400 °C). The peak decomposition into Al-O (blue) and OH/COO (red) are indicated. The measured data and the resulting fitted curve are shown by black (hollow) circles and by black line respectively. Inset shows the C 1s core level spectra of as-deposited and annealed (t_{anl} =105 s, T_{anl} = 400 °C) sample of S_{200}.

yields a high level of chemical passivation after annealing that can be attributed to moderate D_{it} (= 1.3×10^{12} states $eV^{-1}cm^{-2}$).

X-ray photoelectron Spectroscopy (XPS)

XPS being a surface sensitive technique is used to get both qualitative and quantitative information of the stoichiometry and chemical states at the surface. The results of representative as-deposited and annealed (t_{anl} = 105 s, T_{anl} = 400 °C) samples of S_{200} is given here. The survey spectra depict mainly Al and O contributions except carbon contamination (spectra not shown). It is attuned to the C 1s peak position to 285 eV for correction. Figures 6(a) and 6(b) show the Al 2p and O 1s core level spectra respectively of as-deposited and annealed films. These core level spectra are de-convoluted into their Gaussian components to extract the bonding information. In Fig. 6(a), peaks at 74.47 eV and 75.55 eV confirm the presence of Al-O and Al-OH bonds, respectively. The absence of peak at 73 eV which otherwise represents the Al-Al bond suggests that the entire Al is oxidized by the surface-saturation reaction.[46]

In Fig. 6(b), peaks at 531.40 eV and 532.68 eV correspond to Al-O and OH/COO bonds respectively. The existence of OH/COO bonds in thermal Al_2O_3 films are due to the usages of H_2O as oxidant.[47] The elemental ratio of oxygen to aluminum is determined from the peak areas of the Al-O contributions within O 1s and Al 2p core levels. In this case, the contributions from COO and OH groups are not considered. For thicker films, a sensitivity factor is required to calibrate the O/Al ratio from XPS.[13] The resulting $O1s_{Al-O}/Al2p_{Al-O}$ ratio for the as-deposited and annealed film (t_{anl} =105 s) are 1.15 and 1.28 respectively. This shows that the annealed film becomes more oxygen rich than the as-deposited state. The deconvoluted peak areas of Al-O in O 1s and Al 2p spectra of as-deposited and annealed (t_{anl} = 105 s) film of S_{200} are given in Table IV. These values are used to calculate the $O1s_{Al-O}/Al2p_{Al-O}$ ratio. Inset of Fig. 6(b) shows the C 1s core level spectra of

TABLE IV. Deconvoluted peak area of Al-O in O 1s and Al 2p spectra of as-deposited and annealed (t_{anl} = 105 s, T_{anl} = 400 °C) sample of S_{200}.

Peak	As-deposited	Annealed
$O1s_{Al-O}$	5749	5100
$Al2p_{Al-O}$	1394	1111

as-deposited and annealed (t_{anl} = 105 s) sample of S_{200}. This spectra show that the intensity of carbon is less for annealed sample w.r.t. its as-deposited state. This observation is also supported by the decrease in FTIR peak intensity at 2340 cm^{-1} observed in annealed samples w.r.t. it's as-deposited state (S_{200}; Fig. 4(b)). The O-H bonds which are present in neutral charge state[48] decreases in annealed film in O 1s spectra which signifies that there is an increase in oxygen dangling bonds (O_{db}) in annealed state than as-deposited state. Al-OH bond contribution in Al 2p spectra decreases with the annealing which is also support this observation. The increase in O_{db} may suppress the positive fixed charges and activate negative fixed charges in the annealed film. This observation is also supported by the presence of negative fixed charges found in the annealed films estimated using C-V data.

IV. CONCLUSIONS

Silicon surface passivation is studied by thermal ALD deposited Al_2O_3 films deposited at different temperature and annealed for varying time duration. S_{100} film show low refractive index value than S_{200} and S_{300}. For as-deposited films, the lifetime value is comparable for S_{100} and S_{200} whereas τ_{eff} increases for S_{300}. The τ_{eff} value of S_{100} decreases with annealing whereas τ_{eff} increases for S_{200} and S_{300}. The lowest SRV value is realized for films S_{200} and S_{300} which are annealed at 400 °C for 105 s using RTP. However, the total thermal budget of S_{300} is more as compared to S_{200} for the same annealing time and temperature due to higher deposition temperature. The best optimized low thermal budget conditions in terms of deposition temperature & annealing conditions are obtained for S_{200}. C-V measurements show lowest Dit under these annealing conditions. C-V measurement of annealed films of the sample (S_{200}) deposited at 200 °C show that there is an activation of negative fixed charges in these films. XPS study shows that there is a decrease in OH bonds in the O 1s spectra after annealing. This suggests an increase in the oxygen dangling bonds which is responsible for negative charge activation.

ACKNOWLEDGEMENT

The work is carried out under NWP-55 grant from Council of Scientific and Industrial Research, India under TAPSUN initiative. NB, acknowledges CSIR for research fellowship. The authors are thankful to Prof. S.M. Shivaprasad and Mr. Jagdish from JNCASR, Bangalore for XPS measurements.

[1] T. Saga, NPG Asia Materials **2**, 96-102 (2010).
[2] Y. S. Tsuo, P. Menna, T. H. Wang, and T. F. Ciszek, Americam Institute of Physics Conf. Proc. **462**, 453 (1998).
[3] A. V. Shah, H. Schade, M. Vanecek, J. Meier, E. Vallat-Sauvain, N. Wyrsch, U. Kroll, C. Droz, and J. Bailat, J. Prog. Photovolt: Res. Appl. **12**, 113-142 (2004).
[4] B. Hoex, J. J. H. Gielis, M. C. M. Van de Sanden, and W. M. M. Kessels, J. Appl. Phys **104**, 113703 (2008).
[5] B. Hoex, S. B. S. Heil, E. Langereis, M. C. M. Van de Sanden, and W. M. M. Kessels, Appl. Phys. Lett. **89**, 042112 (2006).
[6] G. Agostinelli, A. Delabie, P. Vitanov, Z. Alexieva, H. F. W. Dekkers, S. De Wolf, and G. Beaucarne, Sol. Energy Mater. Sol. Cells **90**, 3438-3443 (2006).
[7] B. Hoex, J. Schmidt, P. Pohl, M. C. M. Van de Sanden, and W. M. M. Kessels, J. Appl. Phys. **104**, 044903 (2008).
[8] K. Matsunaga, T. Tanaka, T. Yamamoto, and Y. Ikuhara, Phys. Rev. B: Condens. Matter Mater. Phys. **68**, 085110 (2003).
[9] Vandana, N. Batra, J. Gope, R. Singh, J. Panigrahi, S. Tyagi, P. Pathi, S. Srivastava, CMS Rauthan, and P. Singh, Phys. Chem. Chem. Physs. **16**, 21804 (2014).
[10] N. Batra, Vandana, S. Kumar, M. Sharma, S Srivastava, P. Sharma, and P. Singh, Sol. Energy Mater. Sol. Cells **100**, 43 (2012).
[11] H. Angermann, W. Henrion, A. Roseler, and M. Rebien, Materials Science and Engineering **B73**, 178-183 (2000).
[12] M. J. Kerr and A. Cuevas, Semiconductor Science and Technology **17**, 35-38 (2002).
[13] G. Dingemans and W. M. M. Kessels, J. vac. Sci. Technol. A. **30**, 040802 (2012).
[14] S. Miyazaki, J. Vac. Sci. Technol. B **19**, 2212 (2001).
[15] K. J. Hubbard and D. G. Schlom, J. Mater. Res. **11**, 2757-2776 (1996).
[16] J. Robertson, J. Vac. Sci. Technol. B **18**, 1785-1791 (2000).
[17] M. Ishida, K. Sawada, S. Yamaguchi, T. Nakamura, and T. Suzaki, Appl. Phys. Lett. **55**, 556 (1989).
[18] P. Saint-Cast, D. Kania, M. Hofmann, J. Benick, J. Rentsch, and R. Preu, Appl. Phys. Lett. **95**, 151502 (2009).
[19] S. Miyajima, J. Irikawa, A. Yamada, and M. Konagai, Appl. Phys. Express **3**, 012301 (2010).
[20] J. Irikawa, S. Miyajima, S. Kida, T. Watahiki, and M. Konagai, Jpn. J. Appl. Phys. **50**, 012301 (2011).

[21] C. Cibert, H. Hidalgo, C. Champeaux, P. Tristant, C. Tixier, J Desmaison, and A. Catherinot, Thin Solid Films **516**, 1290-1296 (2008).
[22] M. T. Seman, D. N. Richards, P. Rowlette, and C. A. Wolden, Chem. Vap. Deposition **14**, 296-302 (2008).
[23] T. T. Li and A. Cuevas, Physica Status Solidi: Rapid Res. Lett. **3**, 160-162 (2009).
[24] G. Seguini, E. Cianci, C. Wiemer, D. Saynova, and J. A. M. Van Roosmalen, Appl. Phys. Lett. **102**, 131603 (2013).
[25] S. M. George, Chem. Rev. **110**, 111-131 (2010).
[26] M. Li, H.-S. Shin, K.-S. Jeong, S.-K. Oh, H. Lee, K. Han, G.-W. Lee, and H.-D. Lee, Journal of Semiconductor Technology and Science **14**, 53 (2014).
[27] A. Dillon, A. Ott, J. Way, and S. George, Surface Science **322**, 230-242 (1995).
[28] M. D. Groner, F. H. Fabreguette, J. W. Elam, and S. M. George, Chem. Mater. **16**, 639-645 (2004).
[29] R. L. Puurunen, J. Appl. Phys. **97**, 121301 (2005).
[30] K. Kukli, M. Ritala, M. Leskela, and Jokinen, J. J. Vac. Sci. Technol. A. **15**, 2214 (1997).
[31] A. W. Stephens and M. A. Green, Sol. Energy Mater. Sol. Cells **45**, 255-265 (1997).
[32] J. Brody, A. Rohatgi, and A. Ristow, Sol. Energy Mater. Sol. Cells **77**, 293-301 (2003).
[33] G. Dingemans, M. C. M. Van de Sanden, and W. M. M. Kessels, Electrochem. Solid-State Lett. **13**, H76-H79 (2010).
[34] G. Dingemans, R. Seguin, P. Engelhart, M. C. M. Van de Sanden, and W. M. M. Kessels, Phys. Status Solidi RRL **4**, 10-12 (2010).
[35] A. Richter, J. Benick, M. Hermle, and S. W. Glunz, Phys. Status Solidi RRL **5**, 202-204 (2011).
[36] J. M. Rafi, M. Zabala, O. Beldarrain, and F. Campabadal, J. Electrochem. Soc. **158**, G108-G114 (2011).
[37] J. Benick, A. Richter, T. T. T. A. Li, N. E. Grant, K. R. McIntosh, Y. Ren, K. J. Weber, M. Hermle, and S. W. Glunz, in *Proc. 35th IEEE PVSC Honolulu*, *Hawaii* (2010).
[38] D. Schuldis, A. Richter, J. Benick, and M. Hermle, in *27th EUPVSEC Frankfurt*, *Germany* (2012).
[39] L. Favaro, A. Boumaza, P. Roy, J. Ledion, G. Sattonnay, J. B. Brubach, A. M. Huntz, and R. Tetot, J. Solid State Chem. **183**, 901-908 (2010).
[40] J. M. Reyes, B. M. P. Ramos, Z. Carlos Islas, W. C. Arriaga, P. R. Quintero, and A. T. Jacome, J. Electrochem. Soc. **160**, B201–B206 (2013).
[41] R. Katamreddy, R. Inman, G. Jursich, A. Soulet, and C. Takoudis, J. Electrochem. Soc. **153**, C701-C706 (2006).
[42] Z. Katz-Tsameret and A. Raveh, J. Vac. Sci. Technol. A. **13**, 1121-1127 (1995).
[43] M. Skotak, Z. Karpinski, W. Juszczyk, J. Pielaszeka, L. Kepinski, D. V. Kazachkin, V. I. Kovalchuk, and J. L. d'Itri, Journal of Catalysis **227**, 11-25 (2004).
[44] D. K. Schroder, *Semiconductor material and device characterization*, 3rd ed. (Wiley-Interscience, Hoboken, NJ, 2006).
[45] G. Dingemans, N. M. Terlindena, D. Pierreuxb, H. B. Profijta, M. C. M. Van de Sanden, and W. M. M. Kessels, Electrochem. Solid-State Lett. **14**, H1-H4 (2011).
[46] J. Koo, S. Kim, S. Jeon, and H. Jeon, Journal of the Korean Physical Society **48**, 131-136 (2006).
[47] J. Haeberle, K. Henkel, H. Gargouri, F. Naumann, B. Gruska, M. Arens, M. Tallarida, and D. Schmeißer, Beilstein J. Nanotechnol. **4**, 732-742 (2013).
[48] B. Shin, J. R. Weber, R. D. Long, P. K. Hurley, C. G. Van de Walle, and P. C. McIntyre, Appl. Phys. Lett. **96**, 152908 (2010).